© 2024 THE BIOPHYSICAL SOCIETY OF JAPAN
Vol. 21, e211018 (2024)
doi: 10.2142/biophysico.bppb-v21.s018

Biophysics and Physicobiology
https://www.jstage.jst.go.jp/browse/biophysico/

Special Issue: Singularity Biology and Beyond

Note (Invited)

Application of single-molecule analysis to singularity phenomenon of cells

Michio Hiroshima[1,2], Hiroko Bannai[3], Gen Matsumoto[4,5], Masahiro Ueda[1,2]

[1] *Laboratory of Single Molecule Biology, Graduate School of Frontier Biosciences, Osaka University, Osaka 565-0871, Japan*
[2] *Laboratory for Cell Signaling Dynamics, RIKEN BDR, Osaka 565-0874, Japan*
[3] *School of Advanced Science and Engineering, Department of Electrical Engineering and Biosciences, Waseda University, Shinjuku-ku, Tokyo 162-0056, Japan*
[4] *Department of Neurological Disease Control, Osaka Metropolitan University Graduate School of Medicine, Osaka 545-8585, Japan*
[5] *Department of Anatomy and Neurobiology, Nagasaki University School of Medicine, Nagasaki 852-8523, Japan*

Received February 29, 2024; Accepted May 2, 2024;
Released online in J-STAGE as advance publication May 8, 2024
Edited by Haruki Nakamura

Single-molecule imaging in living cells is an effective tool for elucidating the mechanisms of cellular phenomena at the molecular level. However, the analysis was not designed for throughput and requires high expertise, preventing it from reaching large scale, which is necessary when searching for rare cells that induce singularity phenomena. To overcome this limitation, we have automated the imaging procedures by combining our own focusing device, artificial intelligence, and robotics. The apparatus, called automated in-cell single-molecule imaging system (AiSIS), achieves a throughput that is a hundred-fold higher than conventional manual imaging operations, enabling the analysis of molecular events by individual cells across a large population. Here, using AiSIS, we demonstrate the single-molecule imaging of molecular behaviors and reactions related to tau protein aggregation, which is considered a singularity phenomenon in neurological disorders. Changes in the dynamics and kinetics of molecular events were observed inside and on the basal membrane of cells after the induction of aggregation. Additionally, to detect rare cells based on the molecular behavior, we developed a method to identify the state of individual cells defined by the quantitative distribution of molecular mobility and clustering. Using this method, cellular variations in receptor behavior were shown to decrease following ligand stimulation. This cell state analysis based on large-scale single-molecule imaging by AiSIS will advance the study of molecular mechanisms causing singularity phenomena.

Key words: single-molecule imaging, large-scale analysis, tau aggregation, single-cell analysis, singularity biology

Significance

AiSIS, a fully automated system for single-molecule imaging and large-scale analysis, revealed the dynamics and kinetics of molecular behaviors and reactions related to tau protein aggregation. This information should benefit the investigation of toxic tau propagation, which is considered a singularity phenomenon in neurological disorders. In addition, a method is shown for identifying the state of individual cells by quantifying receptor mobility and clustering revealed cellular variation, indicating the possibility of identifying outlier cells expressing singularity phenomena.

Corresponding author: Michio Hiroshima, Laboratory of Single Molecule Biology, Graduate School of Frontier Biosciences, Osaka University, 1-3 Yamadaoka, Suita, Osaka 565-0871, Japan. ORCID iD: https://orcid.org/0009-0000-0613-6724, e-mail: m_hiroshima.fbs@osaka-u.ac.jp

Introduction

Single-molecule imaging acquires spatiotemporal information about the dynamics of molecular behaviors and kinetics of molecular reactions in living cells in the endogenous cellular environment. Molecular behaviors on the plasma membrane observed as lateral diffusion, cluster formation, and directed translocation were suggested to depend on signaling processes [1–3]. Based on these analyses, the molecular mechanisms for cellular functions have been elucidated [4–9]. In conventional ensemble assays, average kinetic parameters of molecular reactions are obtained by aligning the starting points of the reactions by mixing solutions of purified molecules in a dedicated device. In single-molecule imaging, the parameters are acquired as distributions, not average values; thus, one can precisely infer the underlying mechanism corresponding to the distribution pattern [6,10,11]. Furthermore, the variance of the parameter distribution can be compared between cells to clarify cellular heterogeneity at the molecular level. Due to its advantageous properties, single-molecule imaging can integrate various pieces of information about signaling protein behavior in a cellular population [12–14].

However, single-molecule imaging has a low throughput and requires sophisticated expertise, complicating the large-scale analysis of cells. Moreover, a molecular event that specifically occurs in a very small number of cells is difficult to measure, making this method unsuitable for observing rare cells that induce a singularity phenomenon. For these reasons, we have automated the imaging processes to improve the throughput and replicate the expertise using an autofocus device with novel optics, artificial intelligence (AI) to search for appropriate cells, and robotics for liquid dispensing [2,15]. This automated in-cell single-molecule imaging system (AiSIS) has imaged 8,000 cells in one day, which corresponds to a 100-fold higher throughput than conventional single-molecule imaging methods.

In Alzheimer's disease (AD), toxic oligomers of tau protein have been suggested to propagate explosively from a small number of cells deep inside the brain to other regions [16], thus acting as a singularity phenomenon. To investigate the molecular mechanism of the propagation, here, we present single-molecule imaging of tau aggregation in the cytoplasm using oblique illumination in AiSIS, which was originally optimized for total internal reflection (TIR) illumination on the basal membrane [2]. Because the tau assembly might influence the plasma membrane, where tau molecules possibly pass through during the propagation [17], the assembled tau might also affect the mobility of membrane proteins. To test this possibility, we assessed the molecular behavior of epidermal growth factor receptor (EGFR), a receptor tyrosine kinase that has been exhaustively studied by single-molecule imaging. Because EGFR behavior has been shown to be sensitive to the membrane environment and correlate with the signaling activity [1,18], our approach may elucidate what and how tau molecules change the membrane as well as the effects of tau assembly on cell signaling [19,20]. Finally, we introduce a method to define individual cellular states based on the parameter distribution of molecular behavior to find rare cells related to the singularity phenomenon.

Materials and Methods

AiSIS: Automated in-cell Single-molecule Imaging System

AiSIS (Figure 1(A)) is based on a normal single-molecule imaging setup: two lasers of wavelengths 488 and 561 nm (OBIS, Coherent) are used to excite green and red fluorescent probes such as GFP and tetramethyl rhodamine (TMR), respectively; an inverted fluorescence microscope (Ti2-E, Nikon) with a 60X or 100X objective lens to focus the light (PlanApo, NA1.49, Nikon); and sCMOS cameras (C15440-20UP, Hamamatsu) to detect the fluorescence. A mirror in the optics is driven by a piezo electric transducer (S-334.2SL1 and E-501.00/E-503.00S/E-509.S3, PI) using a function generator (WF1948, nF) to tilt and rotate the incidence angle of the laser beam for orbicular TIR and oblique illuminations (Figure 1(B)).

For the automated operation of the microscope, a novel autofocus device was used (Figure 1(C)). This device refers to a position of the slit image that is located at the plane optically conjugate to the bottom surface of the cell surface. The slit is illuminated by an 830-nm laser alternately from two angles 180 degrees apart using a Galvano mirror with a frequency of 10 Hz. When the objective is located at in- or out-focus positions, the two slit images are overlapped or move to opposite directions, respectively. Thus, the center of the two images almost corresponds to the in-focus position, and the location of each image reflects the direction and amplitude of the deviation in the focus. Based on this information, the height of the objective lens is feedback-controlled. The difference between the in-focus positions determined by the device and the eyes of the user is adjusted by setting an offset value. This method is robust for variation in the refractive index of the samples, which often induces out-of-focus blur in commercial devices using a laser beam from one direction when the field of view is moved from a blank region to one with a cell in it. The in-focus position is maintained without the influence of any optical blurring by continuous detection of the center of the two slit images.

Another significant procedure in single-molecule imaging is to search for cells in which individual fluorescent spots can be recognized separately (1-3 mm^{-2}) and automatically with deep learning. The neural network constructed for AiSIS is a combination of convolution and deconvolution layers with Rectified Linear Units (ReLU) and sigmoid functions.

Researchers train the neural network in advance by presenting correct and incorrect images that are selected and judged in accordance with their experience. The number of images required for the learning was evaluated using a cross validation to avoid under- or overlearning [2,15]. The output of the neural network was compared with the researcher's answers to images that were and were not used for the network training. Between these images, the average residual square (ARS) was calculated as the root mean of the squared difference between the values of the corresponding pixels in the researcher's answer and the predicted results from the neural network,

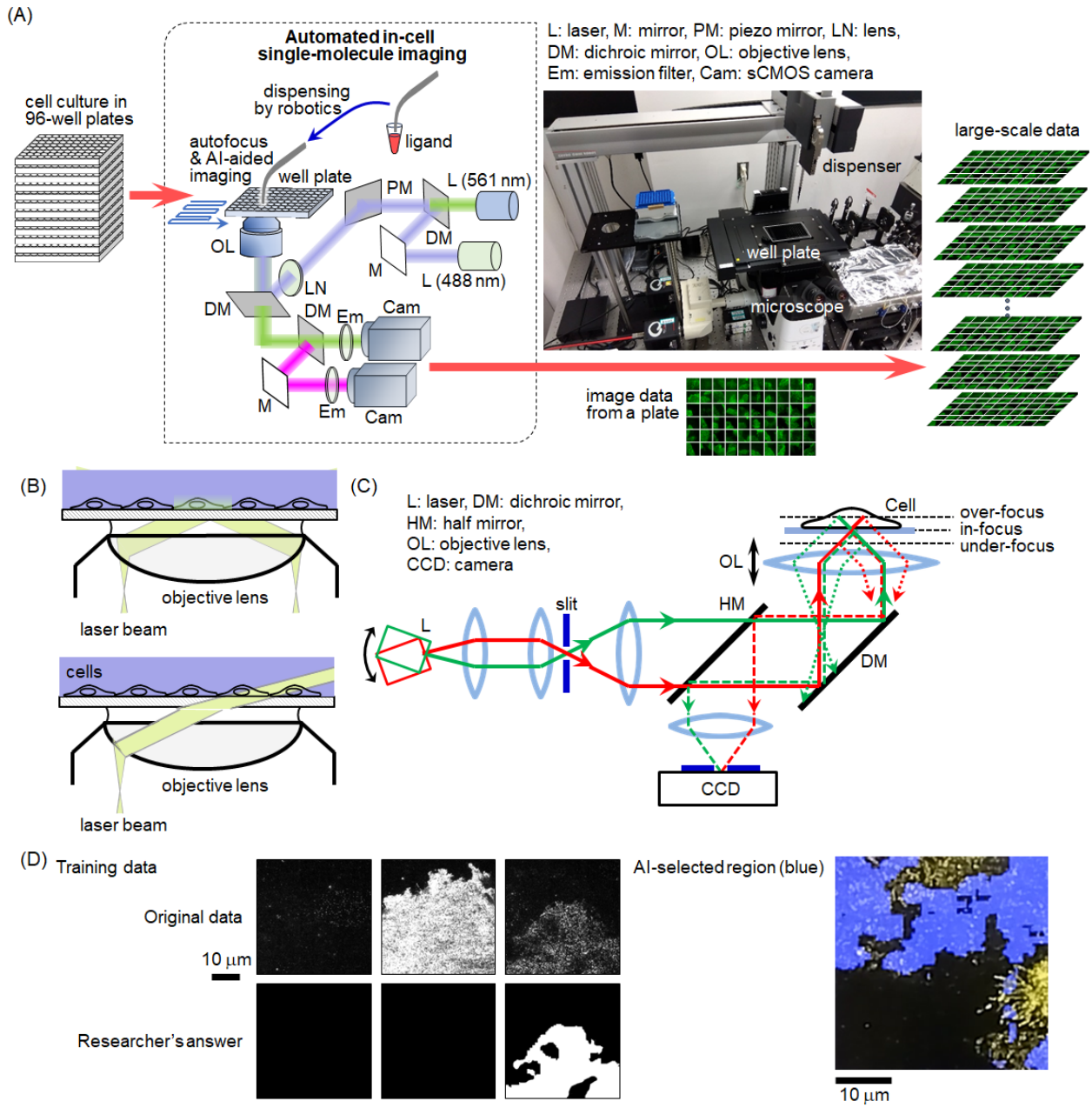

Figure 1 (A) Schematic drawing and photo of AiSIS. (B) TIR (top) and oblique (bottom) illuminations. (C) The autofocus device. (D) AI-aided cell searching. Images used for training the neural network (left) and regions suitable for single-molecule analysis, which were selected by the trained network during the experiment (right).

$$ARS = \sqrt{\frac{1}{512^2}\sum_{i=0}^{511}\sum_{j=0}^{511}\left(y_{i,j} - d_{i,j}\right)^2}$$

Here, $d_{i,j}$ and $y_{i,j}$ are brightness values of pixel (i, j) and $0 \leq i, j < 512$. These values were binarized as 1 for the correct

and 0 for the uncorrected regions that were judged by the researcher/ neural network. When the network has learned well, the ARS was saturated with a value < 0.5. The minimum number of training images was determined to be at least 40. The learned network automatically found suitable cells for the single-molecule analysis during experiments.

Robotics is incorporated into AiSIS for liquid handling (Cavro Omni Robot, Tecan). Solutions of chemicals (e.g., ligands, compounds, and drugs) are sucked from the storage well plate and dispensed into wells in the cell culture plate using set volumes at set timings.

Tau Seed

The recombinant repeat domain of human tau with the P301L mutation (K18-P301L) was used as the tau seed. K18-P301L fragment was expressed in E. coli, purified, and subjected to fibril formation using heparin as described previously [21].

Cell Preparation

A CHO-K1 cell line expressing GFP-tagged epidermal growth factor receptor (EGFR) and a Neuro-2A cell line expressing tau were imaged. Two types of tau proteins were used: OptoTau, which is a P301L mutant human tau protein fused to light-sensitive protein CRY2olig, and OptoTau-ΔN, which is the same as OptoTau but with additional deletions in the N-terminal and proline-rich domains [22]. OptoTau and OptoTau-ΔN were labeled with a SNAP-tag sequence between CRY2olig and tau. In addition, another Neuro-2A cell line expressing SNAP-OptoTau and EGFR-HaloTag was used. CHO-K1 and Neuro-2A cells were cultured in Ham's F-12 and Dulbecco's modified Eagle's media (Wako Chemicals) supplemented with 10% fetal bovine serum. The cell culture was carried out in a 96-well plate (Matsunami GP96000). To induce tau aggregation, two methods were applied: 1) The Neuro-2A cells were illuminated with 0.6 mW/cm^2 blue light of LED (TH2-211X200BL) connected to a power supply (PD3-10024-8-SI(A), CCS) for > 12 hours in 5% CO_2 at 37°C; and 2) 2 mL of tau seed was transfected with Lipofectamine 3000 reagent (Thermo Fisher) and cultured for > 24 hours. In both cases, the culture medium was replaced with DMEM minus phenol red and FBS for starvation 1 day before the experiments, and DMEM was changed to HBSS containing 10 mM HEPES just before the imaging. For the labelling of SNAP-OptoTau, Neuro-2A cells were incubated in DMEM containing 2 and 4 nM SNAP-Cell TMR (tetramethylrhodamine)-Star (S9105S, New England Biolabs), respectively, overnight in 5% CO_2 at 37°C. For the labeling of EGFR-HaloTag, cells were incubated in DMEM containing 20 nM HaloTag TMR ligand (Promega) for 15 min in 5% CO_2 at 37°C.

Single-molecule Analysis

To observe EGFR-GFP on the plasma membrane and SNAP-OptoTau in the cytoplasm, TIR and oblique illuminations were used, respectively. To switch the illumination method, we changed the angle of the piezo mirror (PM) in figure 1(A). For cytoplasm imaging, the angle was decreased such that debris on the surface of the coverslip were not observed and in-focus images of fluorescent tau structures were acquired. Images of 768 × 768 pixels were acquired at a pixel size of 66 nm and frame rate of 30 fps. Automated imaging in AiSIS was operated by Auto Imaging Software (AIS, ZIDO Corp.) to control the autofocus device, AI-aided cell searching, and liquid handling robotics. Single-molecule tracking was applied using Auto Analysis Software (AAS, ZIDO Corp) to obtain the positions (x, y) and intensity (I) of each fluorescent spot in every frame. The positions were used to generate trajectories of individual molecules, and the intensity reflected the size of the clusters.

For every step along the individual trajectories, a hidden Markov model (HMM)-based machine learning method [1,23] inferred a mobility state defined by a diffusion coefficient. In the case of EGFR, three mobility states were suggested. The lateral diffusion was characterized by the mean square displacement (MSD) as follows [1,2,24,25]:

$$MSD(n\Delta t) = [\{x(t + n\Delta t) - x(t)\}^2 + \{y(t + n\Delta t) - y(t)\}^2] \quad (1)$$

where t, Dt, and n indicate time, single-frame period, and number of frames, respectively. [ ] indicates the average. The MSD was calculated for each mobility state.

The resident time of a SNAP-OptoTau molecule in a tau aggregate was obtained as the time duration of each trajectory in the single-molecule tracking data.

Cellular State Analysis

The logarithm of MSD at a lag time of 500 ms (MSD_{500ms}) and average intensity of a trajectory were used to produce two-dimensional (2D) heatmaps consisting of 40X40 matrices representing the probability densities. The heatmaps were obtained for individual cells and compared between the same cells before and after EGF stimulation. To make the EGF-induced changes obvious, differential maps were calculated by subtracting the heatmaps summed over all cells of pre-stimulation from those of post-stimulation, and segmented to several regions by a modified K-means clustering after

smoothing over 3 pixels. When a differential map was divided into N regions described from S_1 to S_N, the centroid of region S_n ($1 \leq n \leq N$) was calculated as

$$\left({u^n}_x,\ {u^n}_y\right) = \left(\frac{\sum_k^{K_n} {x^n}_k \cdot {w^n}_k}{K_n}, \frac{\sum_k^{K_n} {y^n}_k \cdot {w^n}_k}{K_n}\right) \tag{2}$$

where ${u^n}_x$ and ${u^n}_y$ respectively denote the x- and y-positions of the centroid, K_n is the number of sections included in region S_n, and the center of a section in S_n is represented as (x^n_k, y^n_k). w^n_k is the weight function described as follows:

$${w^n}_k = ({P^n}_k)^{1/2} \tag{3}$$

where ${P^n}_k$ is the probability density difference of the section. For each section of the differential map, the distances to all the centroids were calculated. The centroid with the shortest distance was chosen, and the sections choosing the same centroid were put together to configure a renewed region. Then, the centroid of each region was updated using equations (2) and (3), and the following calculations were executed again. This process was iterated until the assignment of all sections to the regions remained unchanged. Before the segmentation, the initial regions were determined by the K-means ++ algorithm. First, the section with the largest absolute value of the probability density difference was set to the centroid of region S_1. Square distances from the centroid to the other sections were calculated as follows:

$${d_{n,i}}^2 = [(x_n - x_i)^2 + (y_n - y_i)^2] \tag{4}$$

where i is the index of the section ranging from 1 to the total number of sections (1600) in the differential map, (x_n, y_n) and (x_i, y_i) denote the centroid of region S_n and the center of the section i, respectively, and $d_{n,i}$ is the distance calculated for all determined centroids. The square distance was converted to weighted values as:

$$D_{n,j} = \frac{w_i \cdot {d_{n,i}}^2}{\sum_j w_i \cdot {d_{n,i}}^2} \tag{5}$$

where w_i is the weight function for section i is described as:

$$w_i = (P_i)^{1/2} \tag{6}$$

where P_i is the absolute value of the probability density difference of the section. Then, the section with the largest $D_{n,i}$ was determined as the centroid of the next region. These processes were executed until the centroid of region S_N was determined. The number of regions, N, was set to 5 according to the number of recognizable regions in the differential map, and the cellular state was defined by the fraction of regions.

Results and Discussions

Tau Association on Tau Aggregates

Single-molecule imaging of TMR-labeled SNAP-OptoTau [22] was carried out inside Neuro-2A cells using oblique illumination by AiSIS (Figure 2(A)). An image with maximum intensity projection along time, which was produced from an acquired 2-sec movie, shows a filamentous structure of tau aggregates when the tau seeds were transfected. The association and dissociation of OptoTau molecules were observed along the filaments, suggesting the exchange of tau molecules between the aggregates and monomers in solution. Without the treatment of tau seeds, no obvious structure was observed, and the rate of association/dissociation seemed faster. Corresponding to these observations, the distribution of residence time for the fluorescent OptoTau spots exhibited a slower decay in cells transfected with tau seeds than those without transfection. Molecular events occurring in the cytoplasm were confirmed at the single-molecule level by AiSIS, although an electric-driven protocol was additionally required to adjust the position of the lens in the autofocus device to observe a higher region in cells where the fixed lens did not work.

Effect of Tau Aggregation on Receptor Mobility

EGFR is a receptor tyrosine kinase and responsible for signal transduction on the plasma membrane after binding to a signal (e.g., ligand) from the extracellular environment. The single-molecule imaging of EGFR on the plasma membrane has been carried out previously [1,4,6] and revealed various behavioral characteristics of EGFR. In those studies, the

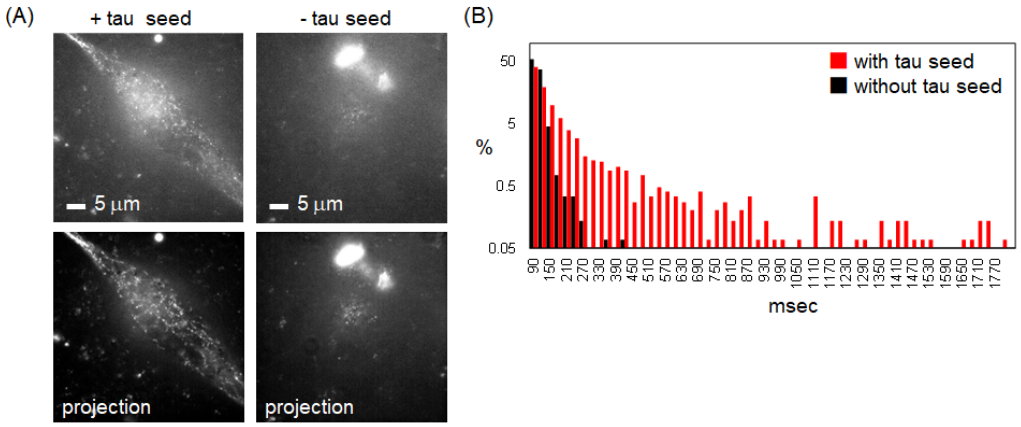

Figure 2 (A) Single-molecule images of Neuro-2A cells expressing OptoTau with (left) and without (right) the transfection of tau seeds. A snap shot (top) and the maximum intensity projection (bottom). (B) Resident times of OptoTau molecules. Red and black bars indicate the distribution with and without the transfection of tau seeds, respectively. The number of measured cells was 1459 for both conditions (with and without tau seed).

mobility was suggested to consist of immobile, slow-mobile, and fast-mobile states according to an HMM-based analysis of single-molecule images obtained with AiSIS. We found that each state exhibits its own diffusion mode: immobile andslow-mobile states as confined diffusion, and a fast-mobile state as free diffusion (Figure 3(A)). The MSD-Dt plot of the confined diffusion was fitted to the following equation [1,2,26]:

$$MSD(t) = \frac{L^2}{3}\left[1 - exp\left(-\frac{12D\cdot\Delta t}{L^2}\right)\right] \tag{7}$$

where D and L are the diffusion coefficient and confinement length, respectively. For the free diffusion, the fitting equation used is

$$MSD(t) = 4D \cdot \Delta t \tag{8}$$

When EGFR is bound to its ligand EGF, phosphorylation occurs in its intracellular domain. During this process, the mobility decreased, as shown by the reduced MSD of slow- and fast-mobile EGFR (Figure 3). The receptor mobility has been reported to be sensitive to the molecular activity, structural change, and membrane environment [1]. To evaluate the effect of tau aggregation on receptors on the plasma membrane, we measured EGFR mobility in Neuro-2A cells expressing SNAP-tagged OptoTau proteins. Blue light illumination onto OptoTau-expressing cells results in the formation of Tau filamentous droplets in the cytosol containing tau oligomers, which are the starting point of Tau aggregation [22]. Figure 3(B) shows the obtained MSD-Δt plot of EGFR in cells with and without the induction of tau droplets by blue light irradiation [27]. When OptoTau was expressed, the confinement length of EGFR diffusion extended regardless of the tau aggregation. Previous studies suggested a direct interaction of both soluble and filamentous tau protein with the plasma membrane especially lipid raft [28,29]. The confinement region for the slow-mobile state was indicated to correspond to a membrane subdomain [1], and the size of which is similar to a lipid raft. The co-localization of EGFR and lipid raft has been indicated by fluorescence imaging at a cellular level [30,31] but not confirmed at the molecular level due to difficulties in imaging lipid molecules in the membrane. EGFR also showed transitions among mobility states; these transitions might correspond to different membrane regions, suggesting that only a partial fraction of EGFR stayed in the raft-like membrane subdomains. At present, the substance of the expanded subdomain in OptoTau-expressing cells is difficult to clarify.

We found that after the droplets were induced, the diffusion mode of EGFR was altered from confined to free (Figure 3(B)). A similar change was observed when membrane cholesterol is depleted [18]. Therefore, OptoTau overexpression and the formation of tau droplets containing tau oligomers might evoke property changes in the plasma membrane and affect the propagation of toxic tau oligomers between cells across the cell membranes in the brains of AD patients. On the other hand, no filamentous structure was observed in OptoTau-ΔN-expressing cells, although some accumulation existed, and the EGFR mobility was no different from that in cells without OptoTau-ΔN expression (Figure 3(B)). The proline rich domain of tau protein has been suggested to promote phase separation and form a condensate in the cytoplasm [32], which is consistent with the results of OptoTau-ΔN-expressing cells in the present study.

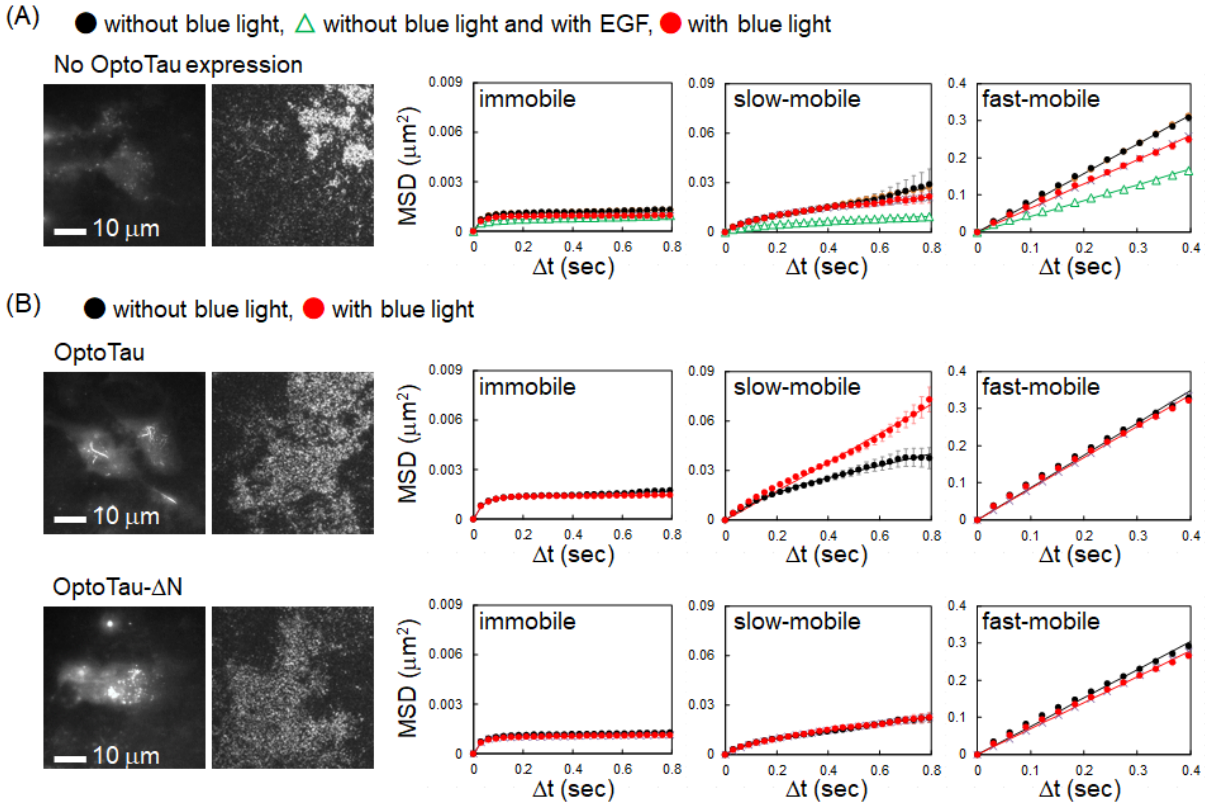

Figure 3 MSD-Δt plots for each mobility state of EGFR in Neuro-2A cells. Left and right photos (different cells) respectively show SNAP-OptoTau in the cytoplasm taken with oblique illumination and TMR-labeled EGFR-HaloTag on the plasma membrane using TIR illumination after blue light irradiation. (A) MSD-Δt plots for cells without OptoTau expression before and after blue light irradiation (21 and 26 cells, respectively). EGF was added to the non-irradiated cells. (B) MSD-Δt plots for cells expressing OptoTau or OptoTau-ΔN before and after blue light irradiation. Circles and triangles are the obtained data, and solid lines indicate the fitting results. The number of measured cells before and after the light irradiation were respectively 18 and 38 for OptoTau and 21 and 26 for OptoTau-ΔN.

Heterogeneity in Cellular States Defined by Receptor Behavior

Single-molecule trajectories of EGFR were obtained both before and after EGF stimulation from the same CHO-K1 cells with AiSIS (Figure 4(A)). 2D heatmaps of MSD_{500ms} (y-axis) and the average intensity (x-axis) [2,3] of the trajectory were produced for a large number of individual cells. The differential map was segmented into five regions, and the individual cellular state was defined by the fraction of the regions in each heatmap. Figure 4(B) shows variation in the cellular states before EGF stimulation, indicating cellular heterogeneity. A previous study indicated a correlation between EGFR slow mobility/high clustering and EGFR phosphorylation [1]; therefore, the variation might reflect differences in the spontaneous or background phosphorylation of EGFR. After EGF stimulation, regions 1 (high mobility) and 5 (low mobility) were on the whole decreased and increased, respectively, depending on the EGF concentration. On the other hand, variations in the fractions of regions disappeared as EGF increased. The cellular state converged in the cell population and approached the state of unstimulated cells with the smallest fraction of region 1 (rightmost column in each EGF condition). Although a plausible mechanism is that the cellular states spanned a wide range of resting cells depending on the EGFR expression level and switched towards the converged distribution upon the maximum activation of all EGFR by EGF stimulation, the correlation between the heterogeneity in receptor behavior and downstream signaling or cell responses remains unknown. AiSIS observations of more signaling molecules under various conditions need to be conducted. We also applied this method to the EGFR behavior observed in Neuro-2A cells expressing OptoTau, which we irradiated with blue light (Figure 4(C)). Like CHO-K1 cells, cellular heterogeneity was seen in these cells in the resting condition but disappeared after the EGF stimulation although a fractions of states was not the same, probably due to difference in cell species.

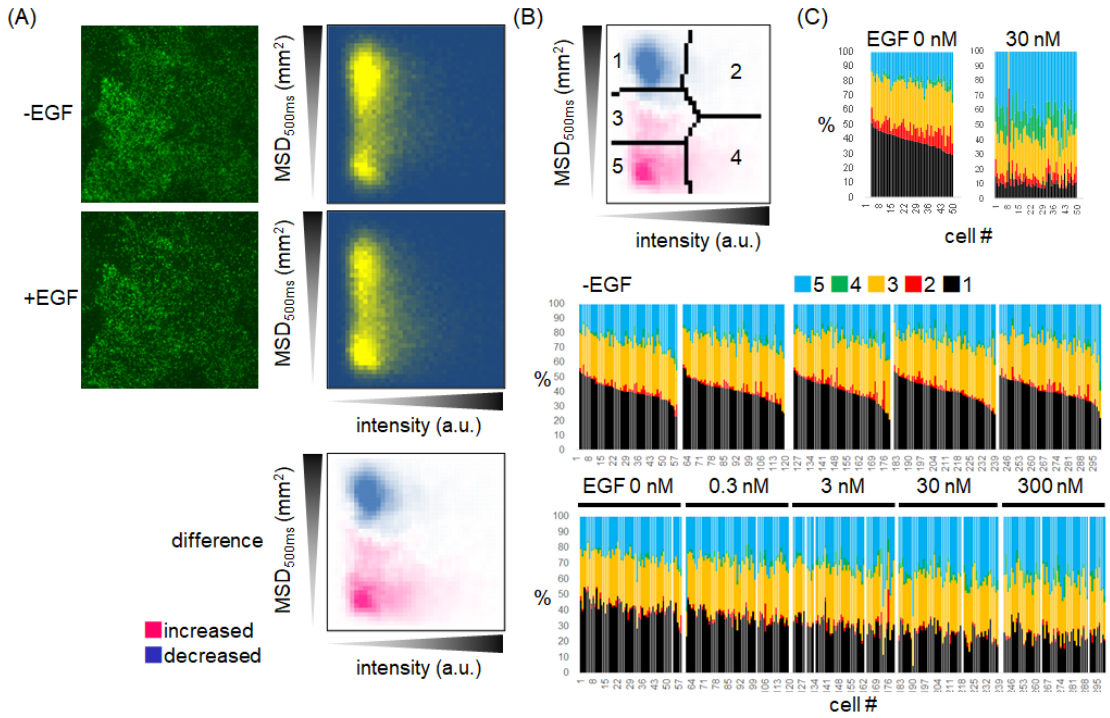

Figure 4 (A) Single-molecule images and 2D heatmaps of EGFR behavior in the same CHO-K1 cell expressing EGFR-GFP before and after EGF stimulation. The heatmaps were summed over all cells. Yellow sections in the heatmaps indicate high probability density. A differential map (bottom) was calculated from the heatmaps. (B) Segmentation of the differential map shown in (A) (top). The fraction of five regions (%) of individual cells (bottom). The same column in the upper and lower graphs correspond to the same cell. Stimulations using the indicated EGF concentrations were applied for 1 min. The number of measured cells was 58 for each EGF concentration. (C) The fraction of five regions (%) of individual Neuro-2A cells expressing SNAP-OptoTau and EGFR-GFP and irradiated with blue light. Cells were different before and after EGF addition (47 and 50 cells, respectively).

Conclusion

Time-consuming manual procedures for single-molecule microscopy, such as focusing, searching suitable cells, recording images, and liquid handling, have been fully automated in AiSIS [2]. This setup has allowed for the large-scale analysis of the behavioral dynamics and reaction kinetics of individual molecules. Using this setup, here, we successfully observed OptoTau proteins at the single-molecule level inside cells by introducing oblique illumination to AiSIS. The OptoTau binding kinetics to filamentous aggregates and the diffusion dynamics of membrane receptors depended on the OptoTau expression, possibly due to tau propagation across the plasma membranes, which is a process of singularity phenomenon in neurological disorders. Furthermore, we present a method to identify individual cellular states based on receptor mobility and clustering. Variations in the cellular state, as defined by EGFR behavior, were observed in the resting condition and decreased with ligand stimulation, suggesting the method can evaluate cellular heterogeneity and find cells with outlier properties in the population. These findings show large-scale single-molecule imaging and analysis using AiSIS is a potent tool to investigate singularity phenomena at the molecular level.

Conflict of Interest

The authors declare no competing interests.

Author Contributions

MH and HB designed the experiments. MH performed the experiments and analyzed the data. HM and GM generated and provided the Neuro-2A cell lines and tau seeds, respectively. MH, HB, GM, and MU wrote the paper.

Data Availability

The data generated and/or analyzed during the current study are available from the corresponding author upon reasonable request.

Acknowledgements

We thank A. Kanayama for providing experimental support, P. Karagiannis for editing the manuscript, and all members of the Ueda lab for discussions. This study is supported by MEXT Japan with Grant-in-Aid for Scientific Research on Innovative Areas (18H05414).

References

[1] Hiroshima, M., Pack, C., Kaizu, K., Takahashi, K., Ueda, M., Sako, Y. Transient acceleration of epidermal growth factor receptor dynamics produces higher-order signaling clusters. J. Mol. Biol. 430, 1386–1401 (2018). https://doi.org/10.1016/j.jmb.2018.02.018

[2] Yasui, M., Hiroshima, M., Kozuka, J., Sako, Y., Ueda, M. Automated single-molecule imaging in living cells. Nat. Commun. 9, 3061 (2018). https://doi.org/10.1038/s41467-018-05524-7

[3] Watanabe, A. D., Hiroshima, M., Ueda, M. Single-molecule tracking-based drug screening. bioRxiv (2023). https://doi.org/10.1101/2023.11.12.566743

[4] Sako, Y., Minoguchi, S., Yanagida, T. Single-molecule imaging of EGFR signalling on the surface of living cells. Nat. Cell Biol. 2, 168–172 (2000). https://doi.org/10.1038/35004044

[5] Ueda, M., Sako, Y., Tanaka, T., Devreotes, P., Yanagida, T. Single-molecule analysis of chemotactic signaling in Dictyostelium cells. Science 294, 864–867 (2001). https://doi.org/10.1126/science.1063951

[6] Teramura, Y., Ichinose, J., Takagi, H., Nishida, K., Yanagida, T., Sako, Y. Single-molecule analysis of epidermal growth factor binding on the surface of living cells. EMBO J. 25, 4215–4222 (2006). https://doi.org/10.1038/sj.emboj.7601308

[7] Matsuoka, S. Single-molecule analysis of chemoattractant-stimulated membrane recruitment of a PH-domain-containing protein. J. Cell Sci. 119, 1071–1079 (2006). https://doi.org/10.1242/jcs.02824

[8] Morimatsu, M., Takagi, H., Ota, K. G., Iwamoto, R., Yanagida, T., Sako, Y. Multiple-state reactions between the epidermal growth factor receptor and Grb2 as observed by using single-molecule analysis. Proc. Natl. Acad. Sci. U.S.A. 104, 18013–18018 (2007). https://doi.org/10.1073/pnas.0701330104

[9] Yasui, M., Matsuoka, S., Ueda, M. PTEN Hopping on the cell membrane is regulated via a positively-charged C2 domain. PLoS Comput. Biol. 10, e1003817 (2014). https://doi.org/10.1371/journal.pcbi.1003817

[10] Taniguchi, Y., Choi, P. J., Li, G.-W., Chen, H., Babu, M., Hearn, J., et al. Quantifying E. coli proteome and transcriptome with single-molecule sensitivity in single cells. Science 329, 533–538 (2010). https://doi.org/10.1126/science.1188308

[11] Hiroshima, M., Saeki, Y., Okada-Hatakeyama, M., Sako, Y. Dynamically varying interactions between heregulin and ErbB proteins detected by single-molecule analysis in living cells. Proc. Natl. Acad. Sci. U.S.A. 109, 13984–13989 (2012). https://doi.org/10.1073/pnas.1200464109

[12] Hibino, K., Shibata, T., Yanagida, T., Sako, Y. Activation kinetics of RAF protein in the ternary complex of RAF, RAS-GTP, and kinase on the plasma membrane of living cells: Single-molecule imaging analysis. J. Biol. Chem. 286, 36460–36468 (2011). https://doi.org/10.1074/jbc.M111.262675

[13] Nakamura, Y., Umeki, N., Abe, M., Sako, Y. Mutation-specific mechanisms of hyperactivation of noonan syndrome SOS molecules detected with single-molecule imaging in living cells. Sci. Rep. 7, 14153 (2017). https://doi.org/10.1038/s41598-017-14190-6

[14] Yoshizawa, R., Umeki, N., Yanagawa, M., Murata, M., Sako, Y. Single-molecule fluorescence imaging of RalGDS on cell surfaces during signal transduction from Ras to Ral. Biophys. Physicobiol. 14, 75–84 (2017). https://doi.org/10.2142/biophysico.14.0_75

[15] Hiroshima, M., Yasui, M., Ueda, M. Large-scale single-molecule imaging aided by artificial intelligence. Microscopy 69, 69–78 (2020). https://doi.org/10.1093/jmicro/dfz116

[16] Holmes, B. B., Furman, J. L., Mahan, T. E., Yamasaki, T. R., Mirbaha, H., Eades, W. C., et al. Proteopathic tau seeding predicts tauopathy in vivo. Proc. Natl. Acad. Sci. U.S.A. 111, E4376–E4385 (2014). https://doi.org/10.1073/pnas.1411649111

[17] Goedert, M., Spillantini, M. G. Propagation of Tau aggregates. Mol. Brain 10, 18 (2017). https://doi.org/10.1186/s13041-017-0298-7

[18] Hiroshima, M., Abe, M., Tomishige, N., Hullin-Matsuda, Françoise Makino, A., Ueda, M., Kobayashi, T., et al.

Membrane cholesterol interferes with tyrosine phosphorylation but facilitates the clustering and signal transduction of EGFR. bioRxiv (2021). https://doi.org/10.1101/2021.08.28.457965

[19] Choi, H. J., Jeong, Y. J., Kim, J., Hoe, H. S. EGFR is a potential dual molecular target for cancer and Alzheimer's disease. Front. Pharmacol. 14, 1238639 (2023). https://doi.org/10.3389/fphar.2023.1238639

[20] Gargini, R., Segura-Collar, B., Herránz, B., Garcia-Escudero, V., Romero-Bravo, A., Núñez, F. J., et al. Tau, downstream of IDH mut, inhibits the EGFR/NF-kB/TAZ mesenchymal axis, normalizing the vasculature and impairing glioma aggressiveness. Sci. Transl. Med. 12, eaax1501 (2020). https://doi.org/10.1126/scitranslmed.aax1501

[21] Matsumoto, G., Matsumoto, K., Kimura, T., Suhara, T., Higuchi, M., Sahara, N., et al. Tau fibril formation in cultured cells compatible with a mouse model of tauopathy. Int. J. Mol. Sci. 19, 1497 (2018). https://doi.org/10.3390/ijms19051497

[22] Soeda, Y., Yoshimura, H., Bannai, H., Koike, R., Takashima, A. Intracellular Tau fragment droplets serve as seeds for Tau fibrils. bioRxiv (2023). https://doi.org/10.1101/2023.09.10.557018

[23] Persson, F., Linden, M., Unoson, C., Elf, J., Persson, F., Lind, M., et al. Extracting intracellular diffusive states and transition rates from singlemolecule tracking data. Nat Methods 10, 265–269 (2013). https://doi.org/10.1038/nmeth.2367

[24] Matsuoka, S., Shibata, T., Ueda, M. Statistical analysis of lateral diffusion and multistate kinetics in single-molecule imaging. Biophys. J. 97, 1115–1124 (2009). https://doi.org/10.1016/j.bpj.2009.06.007

[25] Takebayashi, K., Kamimura, Y., Ueda, M. Field model for multistate lateral diffusion of various transmembrane proteins observed in living Dictyostelium cells. J. Cell Sci. 136, jcs260280 (2023). https://doi.org/10.1242/jcs.260280

[26] Kusumi, A., Sako, Y., Yamamoto, M. Confined lateral diffusion of membrane receptors as studied by single particle tracking (nanovid microscopy). Effects of calcium-induced differentiation in cultured epithelial cells. Biophys. J. 65, 2021–2040 (1993). https://doi.org/10.1016/S0006-3495(93)81253-0

[27] Taslimi, A., Vrana, J. D., Chen, D., Borinskaya, S., Mayer, B. J., Kennedy, M. J., et al. An optimized optogenetic clustering tool for probing protein interaction and function. Nat. Commun. 5, 4925 (2014). https://doi.org/10.1038/ncomms5925

[28] Mammeri, N. El, Gampp, O., Duan, P., Hong, M. Membrane-induced tau amyloid fi brils. Commun. Biol. 6, 467 (2023). https://doi.org/10.1038/s42003-023-04847-6

[29] Cheng, K. H., Graf, A., Lewis, A., Pham, T., Acharya, A. Exploring membrane binding targets of disordered human Tau aggregates on lipid rafts using multiscale molecular dynamics simulations. Membranes (Basel) 12, 1098 (2022). https://doi.org/10.3390/membranes12111098

[30] Zhang, Z., Wang, L., Du, J., Li, Y. Lipid raft localization of epidermal growth factor receptor alters matrix metalloproteinase-1 expression in SiHa cells via the MAPK / ERK signaling pathway. Oncol. Lett. 12, 4991-4998 (2016). https://doi.org/10.3892/ol.2016.5307

[31] Midgley, A. C., Rogers, M., Hallett, M. B., Clayton, A., Bowen, T., Phillips, A. O. Transforming growth factor-β1 (TGF-β1)-stimulated fibroblast to myofibroblast differentiation is mediated by hyaluronan (HA)-facilitated epidermal growth factor receptor (EGFR) and CD44 co-localization in lipid rafts. J. Biol. Chem. 288, 14824-14838 (2013). https://doi.org/10.1074/jbc.M113.451336

[32] Zhang, X., Vigers, M., McCarty, J., Rauch, J. N., Fredrickson, G. H., Wilson, M. Z., et al. The proline-rich domain promotes Tau liquid-liquid phase separation in cells. J. Cell Biol. 219, e202006054 (2020). https://doi.org/10.1083/JCB.202006054

This article is licensed under the Creative Commons Attribution-NonCommercial-ShareAlike 4.0 International License.
To view a copy of this license, visit https://creativecommons.org/licenses/by-nc-sa/4.0/.